New analysis of the radiative decay $\omega \to \eta\gamma$ in proton-antiproton annihilation at rest

T. Case, K. M. Crowe, F. H. Heinsius,* P. Kammel, and M. Lakata
University of California, LBNL, Berkeley, California 94720

T. Degener, H. Koch, M. Kunze, U. Kurilla, H. Matthäy, K. Peters, M. Ratajczak, and H. Stöck
Universität Bochum, D-44780 Bochum, Federal Republic of Germany

B. M. Barnett,† M. Herz, H. Kalinowsky, E. Klempt, B. Pick, C. Straßburger, J. S. Suh, U. Thoma, and K. Wittmack
Universität Bonn, D-53115 Bonn, Federal Republic of Germany

P. Hidas
Academy of Science, H-1525 Budapest, Hungary

C. A. Baker and C. J. Batty
Rutherford Appleton Laboratory, Chilton, Didcot OX110QX, United Kingdom

M. Doser, J. Kisiel,‡ and R. Landua
CERN, CH-1211 Geneva 4, Switzerland

J. Adomeit, J. Meier, R. Ouared, R. Seibert, and U. Strohbusch
Universität Hamburg, D-22761 Hamburg, Federal Republic of Germany

A. Abele, S. Bischoff, P. Blüm, D. Engelhardt, A. Herbstrith, C. Holtzhaußen, and M. Tischhäuser
Universität Karlsruhe, D-76021 Karlsruhe, Federal Republic of Germany

D. V. Bugg, C. Hodd, and B. S. Zou
Queen Mary and Westfield College, London E1 4NS, United Kingdom

R. P. Haddock
University of California, Los Angeles, California 90024

K. Braune, W. Dünnweber, M. A. Faessler, N. P. Hessey, D. Jamnik,§ C. Kolo, W. Roethel, C. Völcker, I. Uman, S. Wallis-Plachner, D. Walther,‖ and U. Wiedner¶
Universität München, D-80333 München, Federal Republic of Germany

A. Berdoz, R. McCrady, and C. A. Meyer
Carnegie Mellon University, Pittsburgh, Pennsylvania 15213

M. Suffert
Centre de Recherches Nucléaires, F-67037 Strasbourg, France

(Crystal Barrel Collaboration)

(Received 4 June 1999; published 4 January 2000)

We report on a measurement of the branching ratio of the rare decay $\omega \to \eta\gamma$ relative to the well known decay $\omega \to \pi^0\gamma$. The ω's are produced in $p\bar{p} \to \eta\omega$ and $p\bar{p} \to \pi^0\omega$. Eigenstate mixing and interference effects of the ω and ρ^0 are taken into account, as well as coherent interference with the background. We find evidence for the non-resonant annihilation channel $B(p\bar{p} \to \eta\eta\gamma) = (3.5 \pm 1.3) \times 10^{-5}$ and limit the value of $B(\omega \to \eta\gamma)$ to the range of $(0.7 \text{ to } 5.5) \times 10^{-4}$ depending on the degree of coherence with the background.

PACS number(s): 13.20.Jf

*Now at University of Freiburg, Freiburg, Germany.
†Now at University of Mainz, Mainz, Germany.
‡Now at University of Silesia, Katowice, Poland.
§Now at University of Ljubljana, Ljubljana, Slovenia.
‖Now at University of Bonn, Bonn, Germany.
¶Now at Uppsala University, Uppsala, Sweden.

I. INTRODUCTION

Radiative meson decays have been used to test various models of nonperturbative QCD, such as the quark model and vector dominance. The family of radiative vector meson to pseudoscalar meson (or vice versa) decays includes 11 different decays. Of these, the decay

$$\omega \to \eta\gamma \tag{1.1}$$

is the focus of this experiment. The decay $\rho^0 \to \eta\gamma$ is also poorly known, but because of the larger ρ^0 width, is more difficult to measure. Because both vector mesons are coherently produced in $p\bar{p}$ annihilation, the measured branching ratio must be corrected for interference and mixing effects, even if the contribution of $\rho^0 \to \eta\gamma$ is small compared to Eq. (1.1) because the cross term in the coherently summed amplitude is significant.

These rare decays were measured relative to the well-known decay $\omega \to \pi^0\gamma$ with a decay branching ratio

$$B(\omega \to \pi^0\gamma) = (8.5 \pm 0.5) \times 10^{-2} \quad [1]. \tag{1.2}$$

We use the ω production channels $p\bar{p} \to \omega\eta$ and $p\bar{p} \to \omega\pi^0$ with

$$B(p\bar{p} \to \omega\eta) = (15.1 \pm 1.2) \times 10^{-3} \quad [2], \tag{1.3}$$

$$B(p\bar{p} \to \omega\pi^0) = (5.73 \pm 0.47) \times 10^{-3} \quad [2]. \tag{1.4}$$

We measure the ratio of events of Eq. (1.1) to the events of Eq. (1.2), where the ω's are produced in the same initial production channel (1.3). The ratio is therefore free of the uncertainty of the branching ratio of Eq. (1.3) or the absolute efficiency of the detector. As a consistency check, we also measure Eq. (1.2) absolutely through both Eqs. (1.3) and (1.4). We consider the neutral decays of η and π^0,

$$\pi^0 \to 2\gamma, \quad \eta \to 2\gamma. \tag{1.5}$$

Thus in both cases the overall process is

$$p\bar{p} \to 5\gamma, \tag{1.6}$$

The main source of background is 6-γ channels from three-pseudoscalar final states ($\pi^0\eta\eta$, $\pi^0\pi^0\eta$ and $\pi^0\pi^0\pi^0$) which can feed through into the 5-γ channels if a soft photon is lost from one of the π^0 decays, i.e., $\pi^0 \to \gamma\gamma_{\rm lost}$.

In addition to this large background, we propose three additional backgrounds, the direct annihilation channels

$$p\bar{p} \to \eta\eta\gamma, \tag{1.7}$$

$$p\bar{p} \to \eta\pi^0\gamma, \tag{1.8}$$

$$p\bar{p} \to \pi^0\pi^0\gamma, \tag{1.9}$$

each described by a constant matrix element, thus appearing flat in the Dalitz plots. The background in Eq. (1.7) can coherently interfere with the desired signal (1.1); in this case the effect is large because both are equal in magnitude. The low statistics and large feed-through background from $\pi^0\eta\eta$ prohibits us from distinguishing this flat background from a similar broad-width background, such as $p\bar{p} \to \sigma\gamma$, $\sigma \to \eta\eta$, where sigma is the very broad $f_0(400-1200)$.

A previous analysis by the Crystal Barrel [3] made the *a priori* assumption that there was no such background. If this channel exists, the previous analysis would not have been able to distinguish the background (1.7) from the signal channel [Eq. (1.3) followed by Eq. (1.1)]. The present analysis, by measuring the ω peak directly, is able to distinguish any nonresonant background from the signal.

II. DETECTOR AND γ RECONSTRUCTION

The data reported here were recorded with the Crystal Barrel detector at LEAR. The detector has been described in detail elsewhere [4], therefore we give only a short description of the relevant components. Antiprotons from the 200 MeV/c LEAR beam were stopped in a liquid hydrogen target and annihilate at rest. The target was surrounded by two coaxial proportional wire chambers, which were only used as a charged particle veto in the trigger. Surrounding the proportional wire chambers was the jet drift chamber (JDC), which was used offline as an additional veto against charged particles. The remaining photons were detected by the surrounding 1380 CsI detectors arranged radially to cover 95% of 4π in $6° \times 6°$ units, and having a resolution of $2.5\%/\sqrt{E[\mathrm{GeV}]^{1/4}}$. The masses of reconstructed mesons have experimental Gaussian sigmas of 8.6 MeV/c^2 for $\pi^0 \to \gamma\gamma$ and 13.4 MeV/c^2 for $\eta \to \gamma\gamma$.

The online trigger required there be no signals in the inner proportional wire chambers, thus selecting ''all-neutral'' events which comprise approximately 3.9% of all $p\bar{p}$ annihilations. 20 million events were accumulated over nine run periods spanning four years.

The photon reconstruction searches for contiguous clusters of fired crystals, requiring the clusters to have a certain minimum energy sum (C1). Within this cluster, each local maximum is considered a separate photon candidate. The highest maximum in a cluster is always considered a photon, while secondary maxima must have at least a certain minimum energy in the central crystal (C2). Finally, an overall threshold (C3) was applied to all resultant photons. These thresholds were necessary to suppress very soft fake photons that were reconstructed due to shower fluctuations at the edges of the clusters.

As we will show, the primary backgrounds come from six photon production sources which lose one photon due to one of the following three mechanisms; (I) a photon below the threshold defined by C1, C2, and C3, (II) a photon shower that merges with another photon shower (conserving total energy and momentum) but reducing the photon multiplicity, or (III) escaping through small gaps in the detector.

The mechanism I is highly sensitive to the set of minima chosen for the photon cuts, while the others are not. Thus to reduce background due to the first mechanism, the three values C1, C2, and C3 were varied until the statistical error quantity $\sqrt{\text{signal}+\text{background}}/\text{signal}$ in the final histograms was minimized, resulting in C1=10.0 MeV, C2=18.0 MeV, C3=11.0 MeV. The events that are due to mechanisms II

TABLE I. Data events surviving each cut. The data is divided into three independent groups at cut 6. A description of each cut is found in the text.

	Cut	Events		
0	All-neutral trigger			20298446
1	0 tracks in JDC			18223703
2	$\lvert p_i\rvert < 200$ MeV/c			13525910
3	$\lvert E-1876\rvert < 200$ MeV			11699206
4	$N_{\gamma=5}$, $E_\gamma > 11$ MeV			748441
5	$4C$ Kin. Fit, $\chi^2/4 < 5$			616155
		$\eta\eta\gamma$	$\eta\pi^0\gamma$	$\pi^0\pi^0\gamma$
6	$6C$ Kin. Fit, $\chi^2/6 < 5$	113546	369689	380479
7	Only 1 solution	5763	136042	204297
8	$6C$ C.L.$>101\%$	2260	93350	128838
9	$m(\gamma_\pi\gamma_r) \notin [80,180]$ MeV/c^2	2146	82349	100369
10	$\gamma_r > 200$ MeV	-	79588	-

and III cannot be directly cut, but are suppressed by the kinematic fit which requires total momentum and energy conservation; only background events with very soft photons can survive.

III. DATA SELECTION

The data cuts are summarized in Table I, and described briefly below. Beginning with 20.3 million all-neutral triggered events, unwanted events with charged tracks are removed. Events with total energy and momentum consistent with annihilation at rest, $p_{\rm tot}=(0,0,0;2m_pc^2)$, where $2m_pc^2 = 1876.54$ MeV, are kept, if the difference for each component is less than 200 MeV/c. These cuts are liberally wide, because a kinematic fit is done in the end. Events with exactly five γ's over 11 MeV are retained.

A kinematic fit is done to the hypothesis,

$$p\bar{p} \to 5\gamma, \tag{3.1}$$

Events were rejected if they fail the $4C$ phase space hypothesis (3.1) with $\chi^2/N_{\rm constraints} > 5.0$, $N_{\rm constraints}=4$ (equivalent to C.L.$<5\times10^{-4}$, see cut 5 in Table I). If the phase space hypothesis succeeded, events were subjected to the following $6C$ hypotheses:

$$p\bar{p} \to \pi^0\pi^0\gamma, \tag{3.2}$$

$$p\bar{p} \to \pi^0\eta\gamma, \tag{3.3}$$

$$p\bar{p} \to \eta\eta\gamma, \tag{3.4}$$

Events must have satisfied at least one of the hypotheses (3.2), (3.3), or (3.4) with $\chi^2/N_{\rm constraints} < 5.0$, $N_{\rm constraints}=6$ (equivalent to C.L.$>4\times10^{-5}$, see cut 6 in Table I). Cut 7 eliminated any event which satisfied two or more of these hypotheses. The $\chi^2/N_{\rm constraints}$ threshold in cut 6 was chosen to be liberally high to identify (and reject) sources of background in cut 7. For example, many events of the type $p\bar{p} \to \eta\omega \to \eta\pi^0\gamma$ which are of type $p\bar{p} \to \pi^0\eta\gamma$ could have also accidentally satisfied the hypothesis $p\bar{p} \to \eta\eta\gamma$. While only reducing the $\pi^0\eta\gamma$ and $\pi^0\pi^0\gamma$ event statistics by a factor of 2, this cut removed about 95% of the events from the $\eta\eta\gamma$ group. After this cut, the three hypothesis groups were disjoint. Cut 8 required a 10% confidence level for the kinematic fit of each group. The last cut helped reject the three pseudoscalar backgrounds which have poor confidence levels due to lost energy from the missing photon.

Confidence levels are directly related to measurement errors and estimated errors of the particles' momentum. Because of varying run conditions, the estimated errors needed to be corrected on a run-period basis. It is necessary to have flat confidence levels for true signal events, for both Monte Carlo simulated events and true data events. The channel $p\bar{p} \to \eta\omega \to \eta\pi^0\gamma$ was chosen for tuning the kinematic fit because it is the strongest signal in the reduced dataset. Since it is impossible to distinguish the signal from background in the data events until the final fit was done, the kinematic fitting and final fitting procedure was iterated, with new scaling factors at each iteration, until the final fit procedure returned a constant branching ratio value independent of confidence level chosen. This correction affects the branching ratio less than 5%.

Some of the background was caused by feed through from wrong pairwise combinations of γ's forming a fake η. Consider the true decay $\omega \to \pi^0\gamma_r \to \gamma_\pi\gamma_\pi\gamma_r$; it is possible that the invariant mass of one of the pairs $\gamma_\pi\gamma_r$ could accidentally be near the η mass (547 MeV/c^2), which would also satisfy the $\omega \to \eta\gamma$ hypothesis. Most of this background was removed by requiring only one solution to the kinematic fit (cut 7). However, it is also possible that the measured invariant mass of $\gamma_\pi\gamma_\pi$ was sufficiently far from the π^0 mass (135 MeV/c^2) that the event would fail the $\omega \to \pi^0\gamma$ hypothesis, and thus not be tagged as background. These events with these ''latent pions'' were removed by rejecting events in which any pairing of the γ_r with the remaining four γ had an invariant mass in the interval [80,180] MeV/c^2 (cut 9). Figure 1 shows the invariant mass of the combination closest to 135 MeV for the $\eta\eta\gamma$ groups of data and of the simulated background channel, $\eta\omega \to \eta\pi^0\gamma$. The simulated $\eta\omega \to \eta\pi^0\gamma$ events showed significant feed through from latent pions, which were removed by cut 9. This latent-pion anticut is discussed again in Sec. VI.

For the $\eta\pi^0\gamma$ group only, the unpaired γ was required to have an energy greater than 200 MeV. This suppressed the small background from the channel $p\bar{p} \to \eta\pi^0$ where a fake fifth γ was caused by a splitoff. However, removal of this background is not so important because it does not influence the measurement of ω's in any case because all events lie near the phase space boundary of the Dalitz plot, far from the ω peak.

The efficiencies for the signal channels as determined by Monte Carlo simulation (see Sec. IV) are $\epsilon(\eta\eta\gamma) = (27.5 \pm 0.8)\%$, $\epsilon(\eta\pi^0\gamma) = (30.0 \pm 0.9)\%$, and $\epsilon(\pi^0\pi^0\gamma) = (25.9 \pm 0.7)\%$ where the errors are statistical.

IV. MONTE CARLO SIMULATED BACKGROUND AND SIGNAL SIMULATION

In this section we describe the procedure for weighting the simulated events for both the background and the signal.

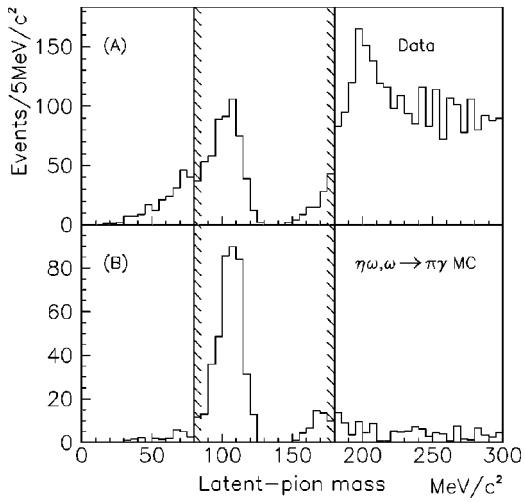

FIG. 1. The invariant mass $m(\gamma\gamma)$ of the best pair which could form a latent pion. (A) is the distribution of the data and (B) is from Monte Carlo simulation of $\eta\omega \to \eta\pi^0\gamma$. Events which fall within the hatched region are removed.

All events were generated flat in phase space using the Crystal Barrel program CBGEANT which is based on GEANT [5].

The two reference channels, $p\bar{p} \to \eta\omega$, $\omega \to \pi^0\gamma$ and $p\bar{p} \to \pi^0\omega$, $\omega \to \pi^0\gamma$, were generated using a nonrelativistic Breit-Wigner parametrization of the ω line shape.

The rare signal channel, $p\bar{p} \to \eta\omega$, $\omega \to \eta\gamma$ coherently interferes with the equally rare $p\bar{p} \to \eta\rho^0$, $\rho^0 \to \eta\gamma$ channel and should coherently interfere with the direct three-body annihilation, $p\bar{p} \to \eta\eta\gamma$, if it exists:

$$p\bar{p} \to \begin{pmatrix} \eta\omega \\ \eta\rho^0 \\ \eta\omega \end{pmatrix} \to \eta\eta\gamma, \tag{4.1}$$

There is no interference from the 4γ or 6γ backgrounds, because these are different final states, and no other significant 5γ channels are known. Even though the overlap between the ρ^0 and ω line shapes (modeled as a Breit-Wigner resonance) is only about 1% of the total integrated ω width, the cross term between the two terms is significant, and can change the net rate $\pm 30\%$ depending on the interference phase and amplitudes. Even more significant is interference with the flat background $\eta\eta\gamma$, whose effect can be up to $\pm 100\%$ depending on the complex phase.

We now discuss how the experimental resolution is folded into the line shape of the omega. For this specific channel, Monte Carlo simulated events for $\eta\eta\gamma$ were generated uniformly in three-body phase space. Each simulated event has two sets of particle momenta, the initial generated momenta and the final reconstructed momenta. The reconstructed momenta are equal to the generated momenta plus smearing due to the detector resolution. Each event is weighted by a dynamic intensity as a function of the initial generated momenta. Since the reconstructed momenta were used in the fits, the reference histograms contain the physical line shape convoluted with the detector resolution. The amplitude is parametrized as a production amplitude A, followed by a propagator which mixes ω and ρ^0 mass eigenstates, followed by a decay amplitude T:

$$S \sim \langle \eta\gamma|T|x'\rangle\langle x'|H|x\rangle\langle x|A|p\bar{p}\rangle, \tag{4.2}$$

where x and x' are mixed states of ω and ρ^0, and the spectator η meson has been suppressed from the equation for clarity. We assume that all the mass-dependent dynamics are contained only in the propagator term Λ, which we parametrize with a mass matrix with off-diagonal terms, δ:

$$A = \left(m - \begin{bmatrix} m_\omega - i\Gamma/2 & \delta \\ \delta & m_\rho - i\Gamma/2 \end{bmatrix} \right)^{-1}, \tag{4.3}$$

$$S = (T_\omega T_\rho)\Lambda \begin{pmatrix} A_\omega \\ A_\rho \end{pmatrix}. \tag{4.4}$$

Thus the net intensity I calculated as

$$I = \sum_{\lambda=\pm 1} |d^1_{1,\lambda}(S_\omega + e^{i\alpha}e^{i\phi}S_\rho) + C_{\rm coh}/\sqrt{2}|^2 + |C_{\rm incoh}|^2, \tag{4.5}$$

$$S_x = \frac{\mu_x}{\sqrt{2\pi}} \frac{|A_x||T_x|}{m - m_x + i\Gamma_x/2} \left(1 - \frac{|A_y|}{|A_x|} \frac{e^{\pm i\alpha}\delta}{m - m_x + i\Gamma_x/2} \right), \tag{4.6}$$

$$|A_x| = \sqrt{B(p\bar{p} \to x\eta)}, \tag{4.7}$$

$$|T_x| = \sqrt{B(x \to \eta\gamma)\Gamma_x}, \tag{4.8}$$

where $x(y)$ is $\omega(\rho^0)$ or $\rho^0(\omega)$. The helicity formalism gives the angular dependence of the ω decay in terms of the rotation matrices, $d^1_{1,\pm\lambda} = (1 \pm \cos\theta)/2$, where λ is the J_z component of the initial $p\bar{p}$ state along the ω momentum axis and θ is the Gottfried-Jackson angle. The decay phase ϕ is the phase difference between the $\omega \to \eta\gamma$ and $\rho^0 \to \eta\gamma$ decays, and is set to zero based on the quark model. The production phase α is the phase difference between the $p\bar{p} \to \eta\omega$ and $p\bar{p} \to \eta\rho^0$ production amplitudes, and is set to zero, based on a Crystal Barrel measurement of this quantity which was consistent with zero [6]. The complex constant $C_{\rm coh}$ describes the coherent contribution of the flat $\eta\eta\gamma$ background to the ω/ρ^0 signal; the real constant $C_{\rm incoh}$ describes the incoherent contribution. The $\pm$ sign in $e^{\pm i\alpha}$ is $+$ for $x = \omega$ and $-$ for $x = \rho$. The mixing parameter is $\delta = 2.5$ MeV [11]. Numerical values for the remaining values are given in Table II [3]. The μ_x are normalization factors, such that the integral over the Dalitz plot of the $|S_x|^2$ with $\delta = 0$ and $\Gamma \to 0$ equals the net branching ratio, $B(p\bar{p} \to X \to \eta\eta\gamma)$. We chose this definition of normalization to be consistent with e^+e^- experiments which generate ω's directly at 781 MeV; i.e., at the nominal mass with an energy spread small compared to the ρ^0 width. There is no further need for an additional amplitude correction when $\Gamma \neq 0$, since the Monte Carlo (MC) simulation, which was generated uniformly in phase space, implicitly generates the mass-dependent acceptance correction. Annihilation branching ratios as determined by the

TABLE II. (Top) Literature branching ratios, used as references for the fits. (Bottom) Parameters used to describe the $(\eta\rho^0 + \eta\omega) \to \eta\eta\gamma$ dynamical intensity.

Process	$B\,(10^{-3})$	Ref.	Process	$B\,(10^{-3})$	Ref.
$p\bar{p} \to \eta\omega$	15.1 ± 1.2	[2]	$p\bar{p} \to \eta\rho^0$	3.9 ± 0.3	[6]
$p\bar{p} \to \pi^0\psi$	5.7 ± 0.3	[2]	$p\bar{p} \to \pi^0\rho^0$	17 ± 3	[7]
$p\bar{p} \to \pi^0\pi^0\pi^0$	6.2 ± 1.0	[8]	$p\bar{p} \to \pi^0\pi^0\eta$	8.2 ± 1.0	[9]
$p\bar{p} \to \pi^0\pi^0\eta\eta$	2.0 ± 0.4	[8]	$p\bar{p} \to \eta\eta$	0.164 ± 0.010	[2]
$\omega \to \eta\gamma$	0.65 ± 0.10	[1]	$\rho^0 \to \eta\gamma$	$0.24^{+0.8}_{-0.9}$	[1]
$\omega \to \pi^0\gamma$	85 ± 5	[1]	$\eta \to \gamma\gamma$	392.5	[10]
Parameter	Value	Ref.	Parameter	Value	Ref.
Γ_ω	8.43 MeV	[10]	Γ_{ρ^0}	150.7 MeV	[10]
$\mu_{\eta\omega}$	771.7 MeV		$\mu_{\eta\rho^0}$	804.0 MeV	
$\mu_{\pi^0\omega}$	1423.0 MeV		$\mu_{\pi^0\rho_0}$	1487.9 MeV	

Crystal Barrel and used in this analysis are integrated over available phase space which may not completely cover the resonance width. In the case of the ρ^0, about 3% of the resonance is outside of phase space. This effect is small enough to be ignored in this analysis, but becomes more significant if resonances are on or near the edge of phase space.

Figure 2 shows an example plot of the theoretical line shape I Eq. (4.5) with $C_{\rm coh} = (3e^{i120^\circ}) \times 10^{-4}$ and the other parameters taken from the best fit discussed later.

The ω and ρ^0 amplitudes are weighted with the proper angular factors for production from ${}^3S_1 p\bar{p} \to \omega\eta$. The angular dependence of the amplitude on the Gottfried-Jackson angle is distributed according to the d functions $d^1_{1,\pm 1} = (1 \pm \cos\theta)/2$ for $J_z = \pm 1$. In the absence of background, these two J_z states are summed incoherently, giving $|d^1_{1,1}|^2 + |d^1_{1,-1}|^2 = 1 + \cos^2\theta$. This distribution was verified by a fit to the angular distribution from $p\bar{p} \to \omega\eta$, $\omega \to \pi^0\gamma$, which is copiously produced and from which the $\pi^0\pi^0\eta$ background can be easily subtracted.

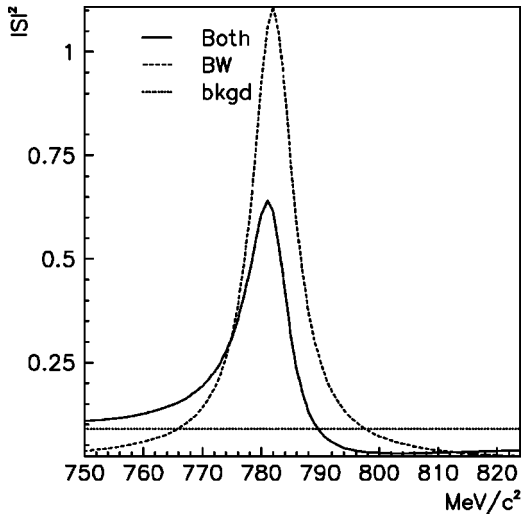

FIG. 2. The solid line ''Both'' is the total intensity I (4.5) of the coherent interference of the ω, ρ^0 and flat background. ''BW'' gives the contribution from $|S_\omega + S_\rho|^2$ and ''bkgd'' gives the contribution from $|C_{\rm coh}|^2$.

The background channels, $\pi^0\eta\eta$, $\pi^0\pi^0\eta$ and $\pi^0\pi^0\pi^0$, are weighted according to the dynamics of each event, taken directly from the high-statistics three pseudoscalar Dalitz plots produced by the Crystal Barrel [8].

V. FITS

The events in the three samples, $\eta\eta\gamma$, $\eta\pi^0\gamma$, and $\pi^0\pi^0\gamma$, were plotted in Dalitz-plot histograms with two-dimensional bins of variable size, and fitted to a linear sum of distributions derived from Monte Carlo simulation of the signal and background channels. Because of limited statistics in both data and Monte Carlo process, the following log-likelihood function was used [12]:

$$-2\ln(L) = 2\sum_j \left(n_j \ln \lambda_j - \lambda_j + \sum_i (m_{ij} \ln f_{ij} - f_{ij}) \right), \tag{5.1}$$

where j runs over the bins of the Dalitz plot, i runs over the MC event samples which represent the constituent parts of the data, n is the number of data events, m is the number of unweighted, reconstructed MC events, f is the *expected* number of unweighted, reconstructed MC events, and λ is the expected number of reconstructed data events, defined as

$$\lambda_j = \sum_i a_i w_{ij} f_{ij}, \tag{5.2}$$

where a_i is the strength of the ith channel and w_{ij} is the additional weight factor (such as angular distribution or dynamical form), normalized to average 1 summed over all j. The method for finding the unknown f_{ij}'s involves a minimization problem for each bin, and the algorithm is given in [12]. The initial values of the a_i are

$$a_{i0} = \frac{b_{\rm trigger} N_{\rm trigger}}{M_i} B(p\bar{p} \to i), \tag{5.3}$$

TABLE III. The final fit values. The errors include internal systematics, but not errors propagated from the literature of the ω intermediate states; see the text.

	No bkgd	Incoh. bkgd	Coh. bkgd
Group $\eta\eta\gamma$			
$B(\omega\to\eta\gamma)\,[10^{-4}]$	3.7 ± 1.1	1.7 ± 1.0	$4.2^{+1.3}_{-1.8}$
$B(p\bar{p}\to\pi^0\eta\eta)\,[10^{-3}]$	2.54 ± 0.08	1.66 ± 0.16	1.80 ± 0.08
$B(p\bar{p}\to\eta\eta\gamma)\,[10^{-5}]$	-	3.4 ± 1.3	3.5 ± 1.3
$\eta\eta\gamma$ phase	-	-	$(130^{+30}_{-10})^\circ$
$-2\ln(L)$	164	131	126
N_{df}	$133-2$	$133-3$	$133-4$
Group $\eta\pi^0\gamma$			
$B(\omega\to\pi^0\gamma)\,[10^{-2}]$	85.9 ± 0.9	88.4 ± 0.9	
$B(p\bar{p}\to\pi^0\pi^0\eta)\,[10^{-3}]$	12.3 ± 1.6	7.1 ± 0.3	
$B(p\bar{p}\to\eta\pi^0\gamma)\,[10^{-4}]$	-	2.5 ± 0.3	
$-2\ln(L)$	2704	2592	
N_{df}	$801-2$	$801-3$	
Group $\pi^0\pi^0\gamma$			
$B(\omega\to\pi^0\gamma)\,[10^{-2}]$	85.0 ± 0.9	85.9 ± 0.9	
$B(p\bar{p}\to\pi^0\pi^0\pi^0)\,[10^{-3}]$	7.0 ± 0.12	6.1 ± 0.12	
$B(p\bar{p}\to\pi^0\pi^0\gamma)\,[10^{-5}]$	-	8.8 ± 0.8	
$-2\ln(L)$	1181	1054	
N_{df}	$424-2$	$424-3$	

where N_{trigger} is the number of triggered data events, b_{trigger} is the all, neutral trigger enhancement $[(3.9\%)^{-1}]$ [13] and M_i is the number of generated events in the ith Monte Carlo simulated data set.

The fitting of each channel's contribution a_i is performed by minimizing the negative log-likelihood with MINUIT [14]. The fit error estimates were done using the MINOS algorithm, or in the case of $B(\omega\to\eta\gamma)$ by inspecting the $\delta(-2\ln(L))=1$ contours.

The list of statistically significant components of the fits is given in Table III. The first fits were done without the flat backgrounds, $\eta\eta\gamma$, $\eta\pi^0\gamma$, or $\pi^0\pi^0\gamma$, in each respective group. The results are shown in the first column of Table III. Some of the small contributions were fixed to the values given in the literature: these include the channels $p\bar{p}\to\eta\omega$, $\omega\to\pi^0\gamma$, $p\bar{p}\to\pi^0\pi^0\eta$, and $p\bar{p}\to\eta\eta$ in the $\eta\eta\gamma$ group; the channel $p\bar{p}\to\pi^0\eta\eta$ in the $\eta\pi^0\gamma$ group; and the channels $p\bar{p}\to\pi^0\pi^0\eta$, $p\bar{p}\to\pi^0\omega\to\pi^0\pi^0\gamma$, and $p\bar{p}\to\pi^0\pi^0$ in the $\pi^0\pi^0\gamma$ group. These contributions are so small that they are omitted from the figures for clarity. The values for $B(\omega\to\eta\gamma)$ and $B(\omega\to\pi^0\omega)$ do not include errors propagated from the literature of the intermediate states $B(p\bar{p}\to\eta\omega)$ or $B(p\bar{p}\to\pi^0\omega)$, which are roughly 10%. This is because this error cancels in the determination of the ratio $B(\omega\to\eta\gamma)/B(\omega\to\pi^0\gamma)$. Most contributions do agree with the literature values in Table II, but the fit contribution of $\pi^0\pi^0\eta$ was 50% higher than expected and is not consistent within the errors; the contributions from $\pi^0\pi^0\pi^0$ and $\pi^0\eta\eta$ were higher too. This is possible evidence that there is an additional background contribution to each channel.

Next, the fits were repeated with inclusion of these flat backgrounds (added incoherently in all cases), and in all cases the log-likelihood improved significantly. Indeed, when this new background is introduced into the fit, the contribution from $\pi^0\pi^0\eta$ drops to a more expected value. Similar results are seen in the $\eta\eta\gamma$ and $\pi^0\pi^0\gamma$ channels.

However, we see a dramatic change in the branching ratio of $\omega\to\eta\gamma$ if the $\eta\eta\gamma$ background is added incoherently. With $C_{\text{coh}}=0$ (allowing only an incoherent contribution from the $\eta\eta\gamma$ background) we find $B(\omega\to\eta\gamma)=(1.7\pm1.0)\times10^{-4}$. This change in the fit is due primarily to the excess of events to the left of the ω peak, which the fit tries to attribute to the $\eta\eta\gamma$ background rather than the low mass tail of the ω resonance.

Since the $\eta\eta\gamma$ background affects the ω peak so strongly, we should properly allow the two to coherently interfere, thus $C_{\text{coh}}\neq0$. There are four real parameters describing the coherent contributions to the ω peak: $B(\omega\to\eta\gamma)$, $B(\rho^0\to\eta\gamma)$ and the magnitude and phase of the complex constant C_{coh} for the $\eta\eta\gamma$ background. Because the fit is not very sensitive to $B(\rho^0\to\eta\gamma)$, we must fix it to the value from Table II. $B(p\bar{p}\to\pi^0\eta\eta)$ and C_{incoh} are allowed to be free in the fit. The remaining values are iteratively scanned in pairs over a suitable range. The log-likelihood plots of the three scans are shown in Fig. 3. The fitted value for C_{incoh} goes to zero when all values are allowed to be free.

The projections of the best fits to the three Dalitz plots are shown in Figs. 4, 5, and 6. The strong ω peaks in the later two plots are well fit, and indeed the fitted values for the $B(p\bar{p}\to\eta\omega\to\eta\pi^0\gamma)$ and $B(p\bar{p}\to\pi^0\omega\to\pi^0\pi^0\gamma)$ agree with each other and to the tabulated values. Figure 4 shows that the fit to the rare ω peak in the reaction $p\bar{p}\to\eta\omega$, $\omega\to\eta\gamma$ is satisfactory. The apparent mass shift of the ω peak by a half bin is not deemed statistically significant.

We have determined the branching ratio of the $p\bar{p}\to\eta\eta\gamma$ direct channel to be

$$B(p\bar{p}\to\eta\eta\gamma)=(3.5\pm0.5_{\text{stat}}\pm1.2_{\text{sys}})\times10^{-5}. \quad (5.4)$$

This value is found to be totally independent of whether the $\eta\eta\gamma$ background is assumed to coherently interfere or not with the ω signal. However, this quantity is correlated to the amount of the $\pi^0\eta\eta$ background, because both backgrounds are relatively broad. The systematic error on this quantity was determined by the variation incurred by either fixing (to the tabulated values in Table II) or releasing the intensity of $\pi^0\eta\eta$ in the fit. The fit favors a phase of C_{coh} of $(130^{+30}_{-10})^\circ$, as seen in Fig. 3. Finally, the branching ratio of $\omega\to\eta\gamma$ is determined to be

$$B(\omega\to\eta\gamma)=4.2^{+1.3}_{-1.8}\times10^{-4} \quad (5.5)$$

from the 1σ contour in Fig. 3.

VI. SYSTEMATICS AND CONSISTENCY CHECKS

An important check of the Monte Carlo simulation is the fit stability versus confidence level. The fit value is constant within 1% for the signal channels, $(\eta\rho^0+\eta\omega)\to\eta\eta\gamma$, $\eta\omega\to\eta\pi^0\gamma$ and $\pi^0\omega\to\pi^0\pi^0\gamma$ as the confidence level is varied from 10% to 100%.

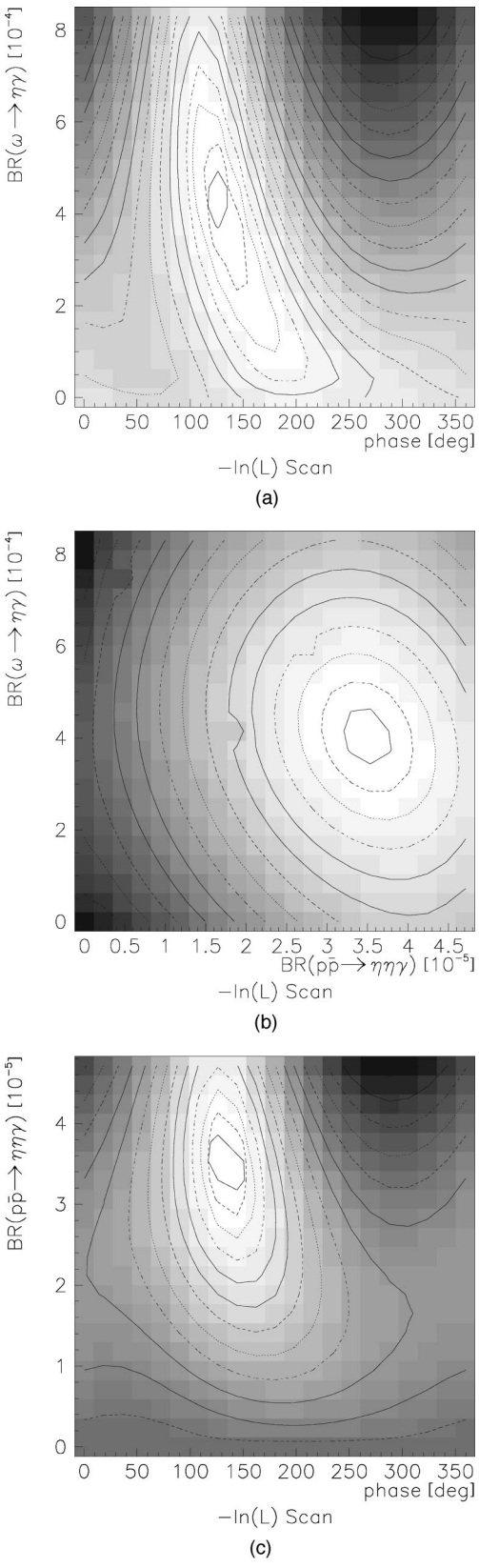

FIG. 3. The contours of $-2\ln(L)$ over a scan of ω parameters. (a) $B(\omega \to \eta\gamma)$ vs phase of $\eta\eta\gamma$, (b) $B(\omega \to \eta\gamma)$ vs $B(\eta\eta\gamma)$, and (c) $B(\eta\eta\gamma)$ vs phase of $\eta\eta\gamma$. Contour lines are drawn at half-sigma intervals; i.e., $-2\ln(L) = -2\ln(L)_{\min} + (i/2)^2$ where i is a positive integer. The second contour line is equivalent to $\Delta\chi^2 = 1$.

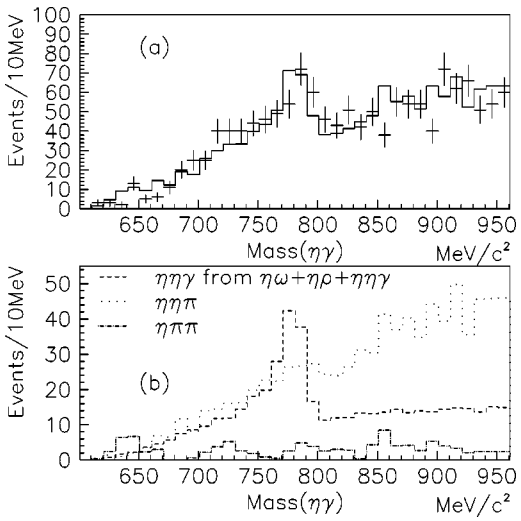

FIG. 4. The $m(\eta\gamma)$ projection of the $\eta\eta\gamma$ Dalitz plot. (a) The data (error bars) and fit result (solid line). (b) The three principle components of the fit, based on Monte Carlo simulation and fitted relative intensities. The coherent $\eta\eta\gamma$ component (dashed histogram) consists of the narrow ω, broader ρ^0, and flat three-body background. Only the ''best'' combination of $\eta\gamma$ whose invariant mass is closest to the ω mass is shown.

If the backgrounds (1.7), (1.8), and (1.9) are omitted, the fit values of the backgrounds from $\pi^0\eta\eta$, $\pi^0\pi^0\eta$, and $\pi^0\pi^0\pi^0$ increase with increasing confidence level, when they should be fixed constants for any cut. This indicates a problem in the characterization of the background. This problem can be eliminated by two methods. The first is to include the backgrounds (1.7), (1.8), and (1.9). With this inclusion, the fit values of the three-pseudoscalar backgrounds remain constant regardless of confidence level cut. The other alternative is to artificially increase the errors input into the kinematic fit by 5–10 % for the three-pseudoscalar channels while keeping the other channels the same. This

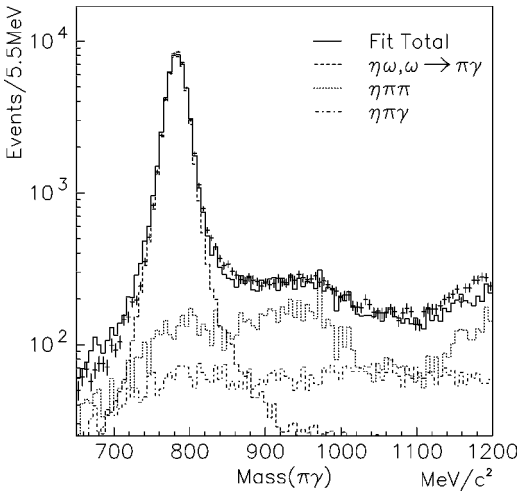

FIG. 5. The $m(\pi^0\gamma)$ projection of the $\eta\pi^0\gamma$ Dalitz plot fit. Shown are the data (error bars) and total fit (solid histogram), superimposed with the three principle components of the fit, $\eta\omega$ (dashed), $\pi^0\pi^0\eta$ (dotted) and $\eta\pi^0\gamma$ (dash-dotted).

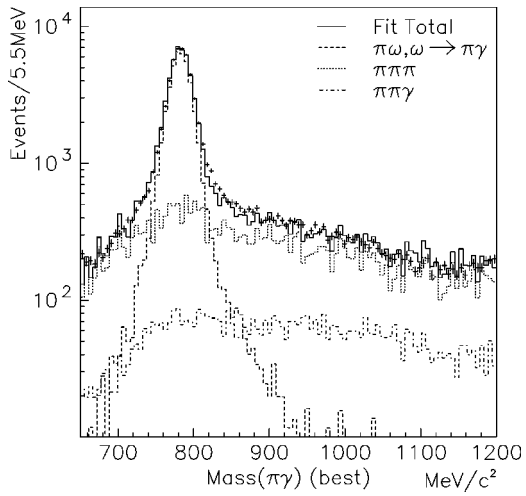

FIG. 6. The $m(\pi^0\gamma)$ projection of the $\pi^0\pi^0\gamma$ Dalitz plot fit. Shown are the data (error bars) and total fit (solid histogram), superimposed with the three principle components of the fit, $\pi^0\omega$ (dashed), $\pi^0\pi^0\pi^0$ (dotted), and $\pi^0\pi^0\gamma$ (dash-dotted). Only the ''best'' combination of $\pi^0\gamma$ whose invariant mass is closest to the ω mass is shown.

achieves a similar satisfactory result, but casts some doubt on the legitimacy of the backgrounds given in Eqs. (1.7), (1.8), and (1.9). Nevertheless, because this untenable problem only appears to affect the backgrounds, we attribute no additional systematic error to the $\omega\rightarrow\eta\gamma$ or $\omega\rightarrow\pi^0\gamma$ measurements.

The only resonant background that can appear under the $\omega\rightarrow\eta\gamma$ peak is leak through from $\eta\omega\rightarrow\eta\pi^0\gamma$, where the π^0 is not identified because of noise (a so-called latent pion, described in Sec. III), and a fake η is formed from a different permutation of the photons of the ω decay. The three photons from the ω decay still reconstruct to the ω mass. It is crucial to thoroughly remove this background channel from the data. To verify that the $\eta\omega\rightarrow\eta\pi^0\gamma$ background was sufficiently suppressed, the width of the latent-pion anticut interval was varied from 10 MeV/c^2 to 170 MeV/c^2. The expected number of leak through events drops to 0 at an interval width of 90 MeV/c^2, and the final result is constant for all widths above 90 MeV/c^2.

The entire analysis was redone with lower γ thresholds (3 MeV cluster threshold, 3 MeV secondary maximum threshold, 20 MeV γ threshold). These low thresholds were chosen to minimize the background from six photon channels, but unfortunately reduced the signal by a large amount, too. There were larger fluctuations in the consistency checks and a larger disagreement with previously published values for the backgrounds. We attribute this to the inaccuracy of the Monte Carlo simulation regarding very soft photon interactions with the barrel. However, the measurement of the $\omega\rightarrow\eta\gamma$ signal was not affected.

To verify that the fit handles bins with low statistics well, the projections of the Dalitz plots where fitted as well. The resultant values were all consistent with the two-dimensional fits within typically 0.5 sigma or less. The statistical errors, however, dominate the final result, so no extra systematic error is added.

VII. DISCUSSION

We discuss why this analysis led to a different result than the previous measurement, and how it is possible that the low value for the number of events in the peak is due to interference effects with the $\eta\eta\gamma$ background.

The previous work [3] relied on the Monte Carlo simulation and previously published branching ratios to calculate the absolute amount of background. It also assumed that there was only one source of background ($\pi^0\eta\eta$). These assumptions could not be directly checked.

The present analysis relies on Monte Carlo simulated data to generate the correct shape of the distributions but does not depend on it to calculate the correct overall efficiency. It does not rely on previously published branching ratios of the six-photon channels to subtract the background. Unforeseen, incoherent broad backgrounds are also not a problem, because the final measurement is based on the ω peak, which floats above all backgrounds and does not depend on the absolute size of the background itself.

The value measured in the earlier analysis of the Crystal Barrel was $B(\omega\rightarrow\eta\gamma)=(6.6\pm1.7)\times10^{-4}$ [3]. Using the same technique as done in this previous analysis but including an incoherent background from $\eta\eta\gamma$ of the same magnitude from the present analysis, we have revised this value to $B(\omega\rightarrow\eta\gamma)=(2.8\pm0.8)\times10^{-4}$ (statistical error only). In the present analysis, if we assume the background is incoherent (see the first column of Table III), we found $B(\omega\rightarrow\eta\gamma)=(1.7\pm1.0)\times10^{-4}$, which is in satisfactory agreement with the revised earlier analysis. This shows that the difference in the two analyses is due primarily to the additional nonresonant background, and not due to a numerical mistake.

The second issue is the reality of the $\eta\eta\gamma$ background. There are four reasons to believe that the flat backgrounds exist. First, the measured branching ratios of all flat backgrounds (see Table III) are small enough to be consistent with a radiative process. An independent partial wave analysis has measured a value of $B(p\bar{p}\rightarrow\pi^0\pi^0\gamma)=(8.8\pm0.7\pm0.6)\times10^{-5}$ [19] which is in good agreement with the result given here. Second, the χ^2 of the Dalitz plot fits of all groups are significantly improved with the addition of this type of flat background (added coherently or incoherently). This argues against the hypothesis that the ''additional'' background is simply due to an incorrect overall efficiency factor of the $\pi^0\eta\eta$ feed-through rate as expected based on the Monte Carlo simulation, because the flat $\eta\eta\gamma$ background does not contain the resonant structure of the $\pi^0\eta\eta$ feed-through background. Third, all the fitted contributions of the backgrounds from the three-pseudoscalar backgrounds ($\pi^0\eta\eta,\pi^0\pi^0\eta,\pi^0\pi^0\pi^0$) become more in line with predictions from published branching ratios when the flat backgrounds are included.

There are two experimental reasons for favoring the hypothesis that the $\eta\eta\gamma$ background interferes coherently rather than incoherently with the ω. First, the $-2\ln(L)$ improves by 5 units (a 2-σ effect), and second, the fit drives the incoherent contribution ($C_{\rm incoh}$) to zero when allowed to be free. Theoretically, all final states arising from the same initial $p\bar{p}$ state interfere coherently, so this is a third reason. In addi-

TABLE IV. Previous measurements of $B(\omega\to\eta\gamma)$ in comparison to this work.

Reference	Reaction	$B(\omega\to\eta\gamma)$ [$\times 10^{-4}$]
[15]	6.7–10 γCu	$3.0^{+2.5}_{-1.8}$
[16]	$e^+e^-\to\omega$	$6.4^{+7.0}_{-4.7}$
[17]	$\pi^-p\to\omega n$	8.3 ± 2.1
[18]	$e^+e^-\to\omega$	$6.6^{+2.4}_{-2.6}$
This work[a]	$p\bar{p}\to\omega\eta$	1.7 ± 1.0
This work[b]	$p\bar{p}\to\omega\eta$	$4.2^{+1.3}_{-1.8}$

[a]With a flat $\eta\eta\gamma$ incoherent background.
[b]With a flat $\eta\eta\gamma$ coherent background.

tion, the result of the coherent hypothesis is greatly favored in comparison to the results of Dolinksy [16], Alde [17], and the recalculation of Alde by Benayoun [18] (Table IV).

In summary, we have corrected our measurement of $B(\omega\to\eta\gamma)$ to account for a flat $\eta\eta\gamma$ background. We have also presented first evidence for the channels $p\bar{p}\to\eta\eta\gamma$ and $p\bar{p}\to\pi^0\eta\gamma$, as well as additional evidence for $p\bar{p}\to\pi^0\pi^0\gamma$.

ACKNOWLEDGMENTS

We would like to thank the technical staff of the LEAR machine group and of all the participating institutions for their invaluable contributions to the success of the experiment. We acknowledge financial support from the German Bundesministerium für Bildung, Wissenschaft, Forschung und Technologie, the Schweizerischer Nationalfonds, the British Particle Physics and Astronomy Research Council, the U.S. Department of Energy and the National Science Research Fund Committee of Hungary (Contract Nos. DE-FG03-87ER40323, DE-AC03-76SF00098, DE-FG02-87ER40315 and OTKA T023635). K.M.C., F.-H.H. and R.O. acknowledge support from the A. von Humboldt Foundation, and N. Djaoshvili from the DAAD.

[1] Particle Data Group, C. Caso *et al.*, Eur. Phys. J. C **3**, 1 (1998).
[2] Crystal Barrel Collaboration, C. Amster *et al.*, Z. Phys. C **58**, 175 (1993).
[3] Crystal Barrel Collaboration, A. Abele *et al.*, Phys. Lett. B **411**, 361 (1997).
[4] Crystal Barrel Collaboration, E. Aker *et al.*, Nucl. Instrum. Methods Phys. Res. A **321**, 69 (1992).
[5] GEANT 3.21 Detector Description and Simulation Tool, CERN program library long writeup W5013, 1994.
[6] Crystal Barrel Collaboration, A. Abele *et al.*, Phys. Lett. B **411**, 354 (1997).
[7] C. Amsler and F. Myhrer, Annu. Rev. Nucl. Part. Sci. **41**, 219 (1991).
[8] Crystal Barrel Collaboration, C. Amsler *et al.*, Phys. Lett. B **355**, 425 (1995).
[9] Crystal Barrel Collaboration, C. Amsler *et al.*, Phys. Lett. B **380**, 453 (1996).
[10] Particle Data Group, R. M. Barnett *et al.*, Phys. Rev. D **54**, 1 (1996).
[11] H. B. O'Connell *et al.*, Phys. Lett. B **354**, 14 (1995).
[12] P. Eberhard *et al.*, Nucl. Instrum. Methods Phys. Res. A **326**, 574 (1993).
[13] Crystal Barrel Collaboration, C. Amsler *et al.*, Phys. Lett. B **311**, 362 (1993).
[14] F. James and M. Roos, CERN-DD long write-up D506, CERN, 1987.
[15] D. Andrews *et al.*, Phys. Rev. Lett. **38**, 198 (1977).
[16] S. Dolinsky *et al.*, Z. Phys. C **42**, 511 (1989).
[17] IHEP-PPLA-LANL-INRU Collaboration, D. Alde *et al.*, Z. Phys. C **61**, 35 (1994).
[18] M. Benayoun *et al.*, Z. Phys. C **72**, 221 (1996).
[19] M. Englert, Ph.D. dissertation, Ludwig-Maximilians-Universität München, 1993.